Physics of the conical broadband terahertz emission from two-color laser-induced plasma filaments

Andrei Gorodetsky,[1,*] Anastasios D. Koulouklidis,[1,2] Maria Massaouti,[1] and Stelios Tzortzakis[1,2,†]

[1]*Institute of Electronic Structure and Laser, Foundation for Research and Technology Hellas, P.O. Box 1527, 71110, Heraklion, Greece*

[2]*Department of Materials Science and Technology University of Crete, P.O. Box 2208, 71003, Heraklion, Greece*

(Received 19 June 2013; revised manuscript received 27 December 2013; published 21 March 2014)

We propose a comprehensive physical model explaining the conical character of broadband terahertz generation from femtosecond two-color laser-induced air plasma filaments. We show, that, in contrast to other models, emission is always conical, resulting from phase matching of the radiation produced inside the filament combined with a partial back reflection of the generated terahertz field from the filament itself due to the frequency-dependent critical plasma density. The obtained conical angle varies from 2° to 10°, depending on the plasma density distribution and filament length. Unlike previously proposed models, our model shows good agreement with our experiments as well as a wide range of experimental findings from the literature.

DOI: 10.1103/PhysRevA.89.033838 PACS number(s): 42.25.Bs, 32.80.Fb, 42.65.Re, 52.38.Hb

I. INTRODUCTION

Since the beginning of the terahertz era in the 1980s, when coherent generation and detection of terahertz (THz) waves was introduced, design and fabrication of more powerful, broadband and controlled THz sources is a question of great importance. Today, the research in this field concentrates mainly on two approaches, both involving the use of ultrashort intense femtosecond laser beams. One focuses on the efficient optical rectification using nonlinear crystals like the $LiNbO_3$ [1] and the second approach is based on the asymmetric photoionization of gases using two-color femtosecond laser filamention [2].

Phase matching (PM) is essential for efficient THz generation in both methods. In the case of optical rectification the main provision for efficient THz generation is to match the THz phase velocity to the group velocity of the optical pulses, that can be achieved either by quasi-PM using periodically poled crystals [3] or noncollinear PM using tilted pulse front excitation [1]. In the two-color plasma generation the total terahertz yield appears to depend on phase matching between the fundamental (ω) and the second (2ω) harmonic of the focused laser beam that produces the filament and hence THz radiation. Since the dephasing length for ω and 2ω in the plasma string for typical average filament plasma densities is about 10–20 mm, it had been considered that no further change in the THz generation from filament elongation can be expected [4]. However, You *et al*. [5] demonstrated continuous increase of the THz yield while changing the filament length up to 60 mm, which is far above the dephasing length. They explain this effect by the THz off-axis PM, i.e., radiation is generated onto a cone surface around the optical axis. Although the THz generation in two-color laser filament model proposed by You *et al*. [5] shows a conical far-field distribution due to THz off-axis PM, it presents a number of inconsistencies and limitations when compared to various experimental findings. This can be understood by a number of parameters that have not been taken into account as well as the fact that the plasma densities considered in their model were far too low ($\sim 10^{16}$ cm^{-3}) compared to the ones in the experiments with measured densities up to $\sim 10^{18}$ cm^{-3} [6]. Other parameters that limited the model were the absence of phase change due to propagation of THz radiation inside the filaments, as well as the fact that all the waves below the plasma frequency cannot propagate through it. Finally, all the calculations in Ref. [5] were performed for monochromatic THz waves, not ultrabroadband as in reality.

Here we propose a comprehensive two-dimensional model of two-color filament THz generation that addresses the shortfalls of the previous model discussed above, like the phase change that terahertz radiation gets due to propagation inside the plasma, as well as plasma opacity for radiation with frequencies below its own one; this gives the opportunity to consider higher plasma density values that are more realistic and close to the experiments. We include the broadband spectral character of the generated terahertz radiation, which in the case of such broadband (0.5–15 THz, i.e., five octaves) radiation is crucial. Also, we introduce spatial nonuniformity of the plasma density both along and across the filament. Following this careful description of the physical processes involved, we show that results obtained with our model compared to Ref. [5] are qualitatively very different. Detailed simulations with full and simplified models for a wide range of initial parameters, if compared with experimentally obtained data of the spatial emission patterns, show much better agreement with our comprehensive approach. Finally, we further validate our model by nicely reproducing other experimental findings from the literature.

II. MODEL

Since the geometry of the process is axially symmetric, we use a two-dimensional model to simplify the equations and speed up the calculations and introduce a flat Cartesian coordinate system with z axis along the filament and x axis across it. THz radiation generated inside the filament is proportional to the nonlinear polarization produced in air by focusing the fundamental and the second harmonic of femtosecond optical pulses:

$$P(x,z,\Omega) \propto A(x,z,\Omega)\sin[\theta(z)]\exp(ik_{THz}z) \qquad (1)$$

*a.gorodetsky@aston.ac.uk

†stzortz@iesl.forth.gr

where $A(x,z,\Omega)$ is the amplitude of the generated terahertz field at a certain point of the filament for all frequencies of interest. The central frequency of the generated spectrum is proportional to the square root of plasma density, as proposed in [2,7–9], and varies from point to point inside the filament, as well as the overall amplitude of the spectrum, which is proportional to the plasma density N_e. The $\sin[\theta(z)]$ term describes the terahertz field amplitude modulation due to the relative phase walk-off between the fundamental and the second harmonic during their propagation inside the filament. For the case of nonuniform filaments, this phase difference can be calculated as

$$\theta(z) = \theta_0 + \int_{z_{\max}}^{z} [n_{2\omega}(z') - n_{\omega}(z')]k_{\omega}dz'. \tag{2}$$

$z_{\max}$ is the coordinate of the point with maximum plasma density inside the filament, $n_{\omega}(z') = n_{\text{air},\omega} + n_{\text{plasma},\omega}(z')$ are the refractive indices for ω and 2ω respectively, $n_{\text{air},\omega,2\omega}$ are taken from [10], and

$$n_{\text{plasma},\omega}(z') \approx \sqrt{1 - \frac{\omega_p^2(z')}{\omega^2}}. \tag{3}$$

To calculate the plasma frequency $\omega_p(z')$ we use the well-known relation [11] $\omega_p = \sqrt{4\pi e^2 N_e(z')/m_e}$, that gives $\sim$1 THz for $N_e = 10^{16}$ cm^{-3}, and $\sim$3 THz for $N_e = 10^{17}$ cm^{-3}.

The last term in Eq. (2) reflects the phase difference of the THz radiation produced at various filament points.

To calculate the THz far-field distribution for a frequency Ω we must integrate over the whole filament with known plasma density distribution [12]:

$$E(r,\Theta,\Omega) \propto k_{THz}\int_V \frac{P(r',\Omega)\exp(ik_{THz}|r-r'|)h(r',r,\Omega)}{|r-r'|}d^2r', \tag{4}$$

where $r = (\xi,\eta)$ is the point at the registration plane, $r' = (x',z')$ is the point inside the filament, and $h(r',r,\Omega)$ represents the phase change that generated THz radiation acquires inside the filament or its blocking if the frequency is less than the plasma frequency at any point of the ray trace between the source point and the registration plane. $h(r',r,\Omega)$ is calculated separately as a multiplier,

$$h(r',r,\Omega) = \begin{cases} 0 & \Omega < \omega_p, \\ \exp\left[i\int_{l(r,r')} k_{THz}[n_{THz}(\xi,\Omega) - 1]d\xi\right] & \Omega \geqslant \omega_p, \end{cases} \tag{5}$$

where $l(r,r')$ is the part of the ray path between r and r' that lies inside the filament (Fig. 1) and n_{THz} is the plasma refractive index at the point ξ on $l(r,r')$ inside the filament for frequency Ω:

$$n_{THz}(\xi,\Omega) = \frac{1}{\sqrt{1 - \frac{\omega_p^2(\xi)}{\Omega^2}}}. \tag{6}$$

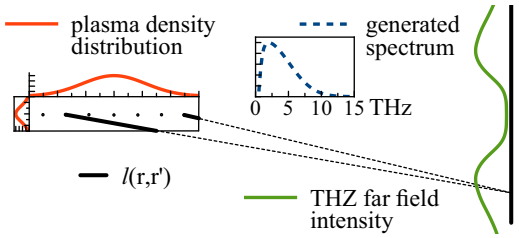

FIG. 1. (Color online) Schematic representation of two-color filament THz generation model.

The unity in Eq. (5) is disregarded not to accumulate the phase change due to wave propagation through the same region in space twice, since it has already been considered in Eq. (4).

The obtained broadband far-field intensity distribution can be then expressed as a sum of monochromatic intensities [13]:

$$I(r,\Theta) = \sum_{\Omega} |E(r,\Theta,\Omega)|^2\alpha(\Omega), \tag{7}$$

where $\alpha(\Omega)$ is the sensitivity function of the detector used in the experiments.

Natural phase matching due to simple interference occurs at various cone angles for all spectral components of the broadband generated spectrum. This results in a broadening of the resulting donut thickness compared to a single wavelength interference pattern. One of the most essential results obtained with this model is the off-axis character of the produced THz for all studied filament lengths and plasma densities starting from a certain minimum peak plasma density $n_{\min}$ which is typically less than 3×10^{14} cm^{-3} and depends on the filament length as shown in Fig. 2(a). Since plasma densities below 3×10^{14} cm^{-3} are much lower than experimentally obtained values [14], we observed conical emission of THz radiation in all studied cases. Extinction of the on-axis emission is explained by the destructive interference of radiation for all wavelengths that appears if phase change of the produced THz wave inside the filament is taken into account [Fig. 2(b)]. The dephasing length of a filament with 7×10^{16} cm^{-3} plasma density is 18 mm, which is almost twice longer than the filament length taken in the model (10 mm). Thus, if in-filament phase change was not considered in the calculations, the produced THz profile would have been on-axis; this is what is shown with the dashed red line in Fig. 2(b). If phase change is introduced, a conical spatial profile appears [solid blue line in Fig. 2(b)]. In Fig. 2(c) we show that even if the conical THz far-field pattern is formed without calculation of the in-filament phase change, because the dephasing length for 7×10^{17} cm^{-3} plasma density is 2.5 mm, eight times less than filament length of 20 mm, phase change addition does not bring any drastic changes on the spatial pattern of the produced THz radiation. These two mechanisms of forming the conical THz emission from the filament also affect the total THz yield slope. For shorter filaments, where the cone is formed mostly by in-filament dephasing, the total THz yield slope is smaller than the one for longer filaments having the same plasma density. For higher plasma densities, the switch between the two mechanisms occurs at shorter filament lengths as can be clearly seen in Fig. 2(e). Also, similarly to [5], the angle of maximum THz intensity direction is bigger for

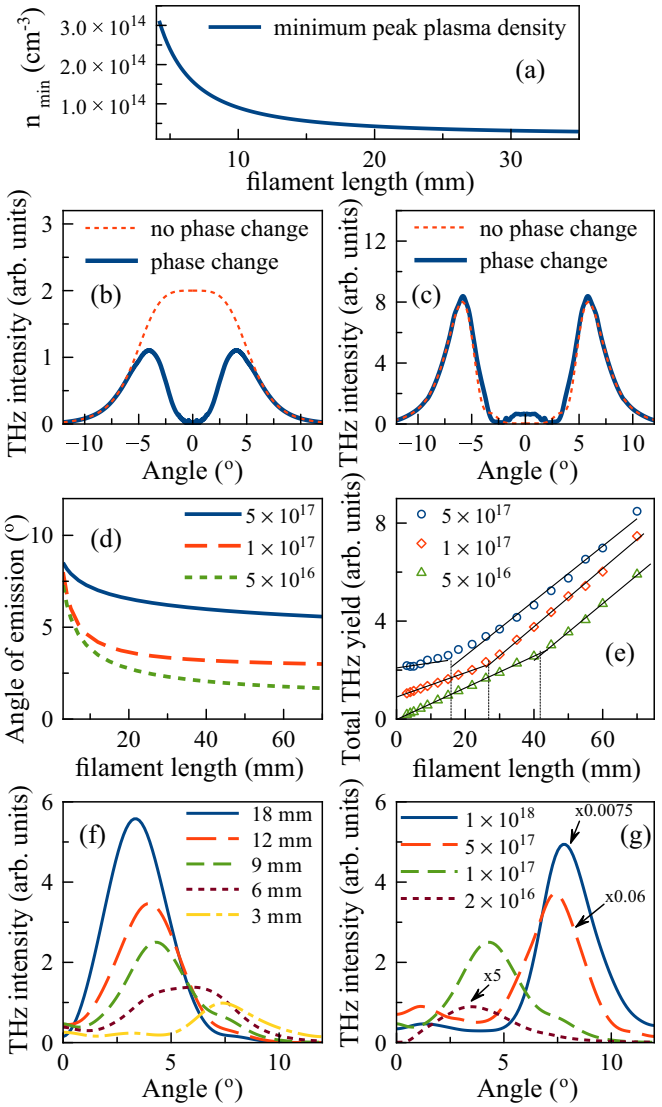

FIG. 2. (Color online) Minimum peak plasma density for conical emission (a), simulation results for far-field THz profiles of 10 mm (b) and 20 mm (c) long filaments with maximum plasma density of 7×10^{16} cm^{-3} and 7×10^{17} cm^{-3} respectively calculated with and without phase change inside the filament, (d) conical emission angle for filaments with different maximum plasma density, (e) total terahertz yield for filaments with different maximum plasma density (scaled and shifted for readability), (f) far-field THz profiles of filaments with maximum plasma density of 1×10^{17} cm^{-3} and different lengths, (g) far-field THz profiles of 9-mm-long filaments with various maximum plasma densities, scaled to fit the plot, multipliers shown with arrows.

higher plasma densities [Fig. 2(g)], but at the same time shorter filaments, even with the same plasma densities produce wider cones of generated THz radiation [Fig. 2(f)]. If we plot the conical angle versus filament length, we can see a clear and obvious dependency from both plasma density and filament length [Fig. 2(d)]. In all graphs, the mentioned plasma density value corresponds to the filament's maximum plasma density while considering, in general, a Gaussian plasma distribution along and across the propagation axis [6].

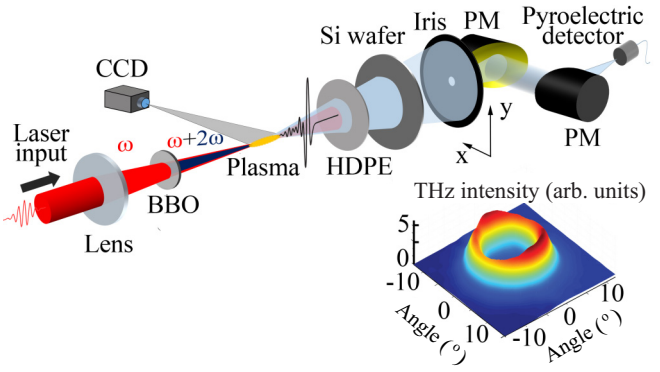

FIG. 3. (Color online) Experimental setup for two-color plasma terahertz generation and far-field THz beam profiling; inset: measured conical profile of the THz emission from two-color plasma filament. PM: parabolic mirror, HDPE: high density polyethilene filter, BBO: β barium borate type-I crystal. Inset shows measured THz profile.

III. EXPERIMENT

In order to validate our theoretical predictions, we have performed experiments using the setup shown in Fig. 3. A Ti:sapphire chirped-pulse amplification laser system delivering 35-fs, 800-nm IR pulses with energies up to 30 mJ at 50-Hz repetition rate has been used. The pulse energy of the beam was controlled by the amplifier of the laser to the desired value. The fundamental (ω) beam was focused by an $f = 200$-mm lens followed by a 50-μm-thick β-barium borate (BBO) type-I crystal, cut at 29.9°, which generates its second harmonic (2ω).

Both ω and 2ω were focused in ambient air creating a plasma filament around the focal point that generates THz radiation. A 3-mm-thick HDPE filter followed by a 1.5-mm Si wafer were used to filter out any optical and residual IR radiation. In order to obtain the spatial profile of the THz beam an iris of 2 mm in diameter was placed 110 mm away from the end of the filament and was scanned in the x-y plane using a two-dimensional (2D) motorized stage allowing for a 50 × 50-mm scanning range. The radiation transmitted through the iris was collected and guided by two parabolic mirrors onto a broadband pyroelectric detector as shown in Fig. 3.

To tailor the plasma strings and control their uniformity we appropriately adjusted the input laser pulse energy as well as the beam wave front, introducing astigmatism and wavefront distortions by tilting the focusing lens. In this way, different plasma string profiles (both symmetric and asymmetric) with different lengths and maximum electron densities were created. In each case, both THz patterns and plasma spatial distributions were recorded. The spatial distribution of the generated plasma was recorded using a linear charge-coupled device (CCD) camera and imaging its fluorescence emission, providing an estimation for the plasma electron density based on previous measurements and works with our system [6,14]. In all the experiments the recorded profile of the produced THz radiation had a conical spatial intensity distribution (inset in Fig. 3).

Our experiments can be grouped in two cases. In the first one we studied the evolution of the THz beam profile changes

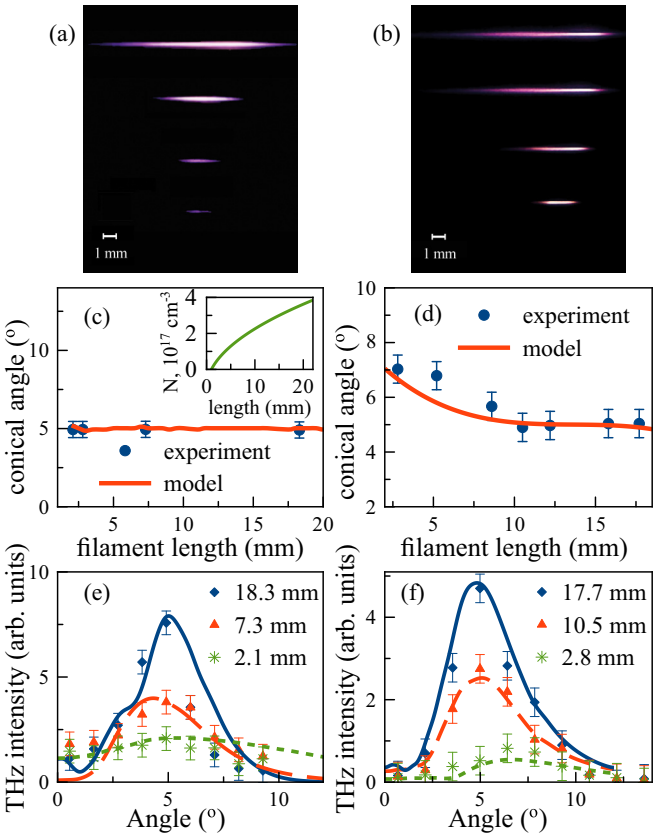

FIG. 4. (Color online) Terahertz generation in symmetric (a), (c), (e) and asymmetric (b),(d), (f) plasma density distribution filaments: (a), (b) — photo of filaments, (c),(d) — conical angle of generated THz, blue points represent experimental results, lines show simulation results, (e),(f) — far field THz intensity profiles produced by filaments shown in (a) and (b) respectively. Dots represent experimental results and lines show simulation results. The inset in (c) shows the maximum plasma density dependency vs. length used in the model for this specific figure.

when decreasing the filament"s maximum electron density and symmetrically shortening its length; see corresponding filament profiles in Fig. 4(a). This was achieved by just reducing the input laser power. In the second case the maximum electron density remained constant while the filament's length was getting shorter but in an asymmetric way this time, as shown in Fig. 4(b). This result was achieved by reducing the input power and in parallel appropriately tilting the focusing lens.

Our experimental results together with corresponding simulations from our model are shown in Fig. 4. In Figs. 4(c) and 4(d) we plot the corresponding conical angle vs filament length dependency for the cases of Figs. 4(a) and 4(b) respectively. For the simulation results shown in Fig. 4(c) both the filament length and peak plasma density were varied as shown in the inset of Fig. 4(c). In contrast, for the simulations in Fig. 4(d) the peak electron density was kept fixed, at 3×10^{17} cm^{-3}, while reducing the filament asymmetric Gaussian distribution length. Experimental and simulated far-field THz patterns for selected points from Figs. 4(c) and 4(d) are shown in Figs. 4(e) and 4(f) respectively. From these one can see that not only the angle of maximum

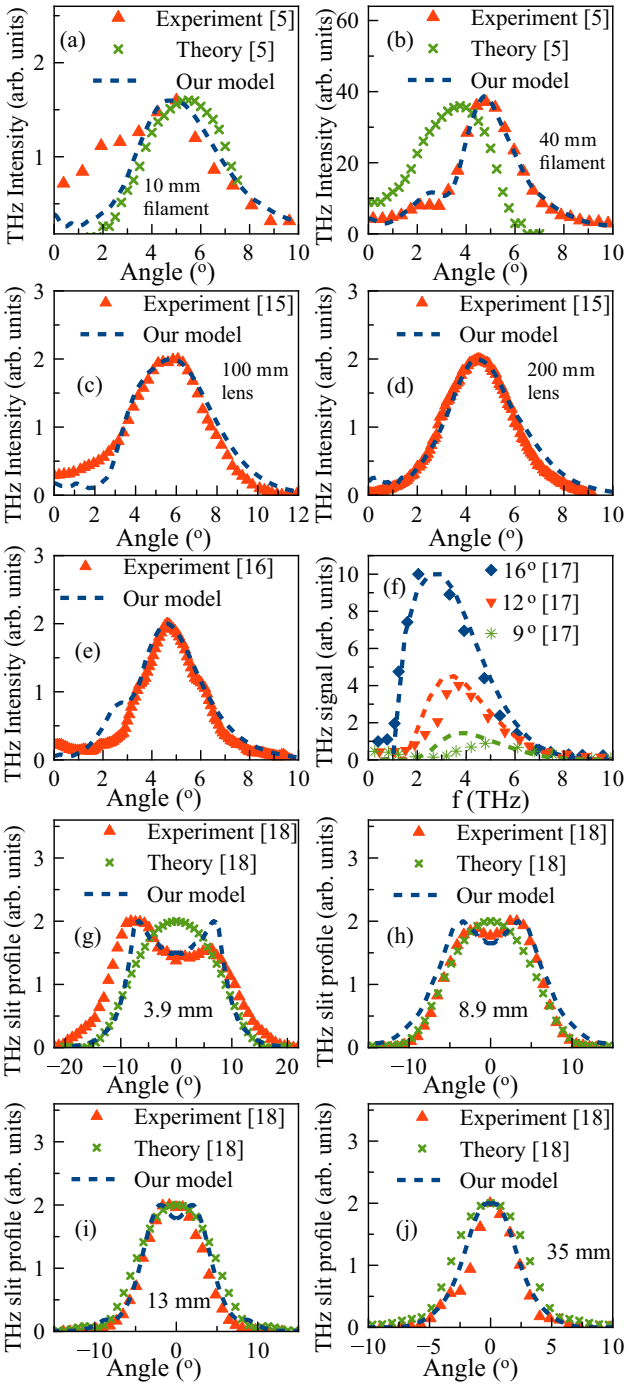

FIG. 5. (Color online) (a),(b) Far-field THz patterns through germanium filter, experimental (triangles) and theoretical (crosses) points taken from [5] and compared with our model (dashed line), for two cases of (a) 10-mm filament produced by 1.3-mJ pulse, (b) 40-mm filament produced by 5-mJ pulse; (c),(d) far-field THz patterns: experimental points (triangles) taken from [15] and compared with our model (dashed line), for two cases of (c) filament produced through 100-mm lens, (d) filament produced through 200-mm lens, pulse energy in both cases 0.71 mJ; (e) far-field THz pattern from [16] repeated and explained with our model (dashed line); (f) simulated THz spectra for various collection angles, experimental data taken from [17], followed by dashed lines calculated with our model; (g)–(j) THz patterns from [18] (triangles), with their theory (crosses) and reproduced with our model (dashed line).

emission, but also the shapes and absolute values of these curves match, demonstrating the strength of our model.

IV. COMPARISON WITH EXPERIMENTAL DATA FROM LITERATURE

To further check our model we also explored other experimental works from the literature. First, we used results of far-field THz mapping obtained by You *et al.* [5]. For the simulations we used the filament lengths they report. As for the plasma densities, based on our past works and experience [6,14] and taking into account the lenses and pulse energies they use, we estimate that the maximum plasma density should not be less than 10^{17} cm^{-3}. For our simulations, we used a plasma density of 10^{17} cm^{-3} for the 10-mm filament and 2.5×10^{17} cm^{-3} for the 40-mm filament respectively. As can be seen in Figs. 5(a) and 5(b), our simulations are in better agreement than their own theoretical predictions.

In other recent works by Blank *et al.* [15] and Klarskov *et al.* [16] conical emission from two-color filaments was demonstrated, and in [15] the same filament tailoring by tuning the laser pulse energy was performed as we described above with very similar results. In their experiments the THz generation cone angle remained constant for all pulse energies, something that surprised the authors of that paper but is naturally explained by our model as presented in Figs. 4(a), 4(c), and 4(e). It is worth noticing once more that in order not to block on-axis radiation by photocarriers induced in silicon filters, we use a HDPE filter put in front of the silicon wafer. To reproduce experimental results from [15] we took the filament length of 9.5 mm with maximum plasma density of 5.5×10^{17} cm^{-3} for a 100-mm lens [Fig. 5(c)] and the filament length of 14 mm with maximum plasma density of 1.8×10^{17} cm^{-3} for a 200-mm lens [Fig. 5(d)]. For the THz emission profile from [16] reproduction, we took the filament length of 22 mm, which is close to the length they report, and a plasma density of 3×10^{17} cm^{-3}, estimated from the pulse energy they use. A comparison of the experimental data from [16] with our model results is shown in Fig. 5(e).

Our model describes not only the spatial profile of the generated THz field, but also its spectrum. In another recent work Borodin *et al.* [17] studied the conical emission from two-color filaments and showed that higher THz frequencies are found at smaller cone angles. We have performed simulations with our code for their experiments and as can be seen in Fig. 5(f), we find nice agreement between their experiments and our model for the spectral distribution. In the model, we used a peak electron density of 1.5×10^{17} cm^{-3}, which is close to the average one they report, and a filament length of 7 mm, which is in agreement with our measurements under similar experimental conditions; Fig. 4(c). Finally, we reproduced some older experimental data from Ref. [18]. For this we rearranged our model output to show the result of scanning the THz profile with a vertical slit. We used the filament lengths given in [18], yet for the plasma densities we again use our estimations. Thus we used THz profiles for a $3.9\times$ 0.2-mm filament with 8×10^{16}-cm^{-3} maximum plasma density, Fig. 5(g), a 8.9×0.36-mm filament with 3×10^{16}-cm^{-3} maximum plasma density, Fig. 5(h), a 13×0.2-mm filament with 2×10^{16}-cm^{-3} maximum plasma density, Fig. 5(i), and a 35×0.08-mm filament with 6×10^{15}-cm^{-3} maximum plasma density, Fig. 5(j). As can be clearly seen, also in these cases our model describes the experimental findings nicely and better than previously mentioned models. Another approach to the explanation of the conical emission suggested in Ref. [19] also predicts off-axis only THz generation.

V. CONCLUSION

We propose a comprehensive physical model for the off-axis phase-matched THz generation in two-color filamentation. In particular, this model allows working with realistic plasma densities, includes the broadband nature of THz pulses from filaments, and shows very good agreement not only with our experimental results, but also with many other experimental results in the literature. For all combinations of filament lengths and realistic maximum plasma densities the far-field THz distributions have a donutlike shape, which is a theoretical result confirmed by experiments. The angle of the conical emission drops with decreasing plasma electron density or increasing filament length. The total THz yield increases almost linearly with filament length, thus the THz output can be effectively increased by extending the filament length with a constant plasma density. Finally, the fact that lower THz frequencies find themselves at bigger cone angles allows one to use this effect for spatially tuned spectral filtering of the plasma filament generated THz radiation.

ACKNOWLEDGMENTS

This work was supported by the Aristeia project FTERA (Grant No. 2570), co-funded by the European Social Fund (ESF) and National Resources. We also acknowledge support from the EU projects "Laserlab III" and "Charisma." A.G. thanks Magicplot Systems, LLC, for providing MagicPlot Pro cross-platform plotting software used for preparation of all figures in the paper except Fig. 3.

[1] J. Hebling, K. L. Yeh, M. C. Hoffmann, and K. A. Nelson, IEEE J. Sel. Top. Quantum Electron. **14**, 345 (2008).

[2] K. Y. Kim, A. J. Taylor, J. H. Glownia, and G. Rodriguez, Nat. Photon. **2**, 605 (2008).

[3] Y.-S. Lee, T. Meade, V. Perlin, H. Winful, T. B. Norris, and A. Galvanauskas, Appl. Phys. Lett. **76**, 2505 (2000).

[4] Y. Liu, A. Houard, M. Durand, B. Prade, and A. Mysyrowicz, Opt. Express **17**, 11480 (2009).

[5] Y. S. You, T. I. Oh, and K. Y. Kim, Phys. Rev. Lett. **109**, 183902 (2012).

[6] J.-M. Manceau, A. Averchi, F Bonaretti, D. Faccio, P. Di Trapani, A. Couairon, and S. Tzortzakis, Opt. Lett. **34**, 2165 (2009).

[7] C. D'Amico, A. Houard, S. Akturk, Y. Liu, J. Le Bloas, M. Franco, B. Prade, A. Couairon, V. T. Tikhonchuk, and A. Mysyrowicz, New J. Phys. **10**, 013015 (2008).

[8] P. Sprangle, J. R. Penano, B. Hafizi, and C. A. Kapetanakos, Phys. Rev. E **69**, 066415 (2004).
[9] M. Chen, A. Pukhov, X. Y. Peng, and O. Willi, Phys. Rev. E **78**, 046406 (2008).
[10] B. Edlén, Metrologia **2**, 71 (1966).
[11] N. A. Panov, O. G. Kosareva, V. A. Andreeva, A. B. Savelev, D. S. Uryupina, R. V. Volkov, V. A. Makarov, and A. P. Shkurinov, JETP Lett. **93**, 638 (2011).
[12] J. W. Goodman, *Introduction to Fourier Optics*, McGraw-Hill Physical and Quantum Electronics Series (McGraw-Hill Book Co., New York, 1968).
[13] A. Gorodetsky and V.G. Bespalov, SPIE Proc. Ser. **7601**, 760107 (2010).
[14] D. Abdollahpour, S. Suntsov, D. G. Papazoglou, and S. Tzortzakis, Opt. Express **19**, 16866 (2011).
[15] V. Blank, M. D. Thomson, and H. G. Roskos, New J. Phys. **15**, 075023 (2013).
[16] P. Klarskov, A. C. Strikwerda, K. Iwaszczuk, and P. U. Jepsen, New J. Phys. **15**, 075012 (2013).
[17] A. V. Borodin, M. N. Esaulkov, I. I. Kuritsyn, I. A. Kotelnikov, and A. P. Shkurinov, J. Opt. Soc. Am. B **29**, 1911 (2013).
[18] H. Zhong, N. Karpowicz, and X.-C. Zhang, Appl. Phys. Lett. **88**, 261103 (2006).
[19] L. A. Johnson, J. P. Palastro, T. M. Antonsen, and K. Y. Kim, Phys. Rev. A **88**, 063804 (2013).